

PAPER

The formation and stability of junctions in single-wall carbon nanotubes

To cite this article: Xiuyun Zhang *et al* 2018 *Nanotechnology* **29** 485702

View the [article online](#) for updates and enhancements.




IOP | ebooksTM

Bringing you innovative digital publishing with leading voices to create your essential collection of books in STEM research.

Start exploring the [collection](#) - download the first chapter of every title for free.

The formation and stability of junctions in single-wall carbon nanotubes

Xiuyun Zhang^{1,2,4} , Jichen Dong², Xiaoshu Gong¹ and Feng Ding^{2,3,4}

¹ College of Physics Science and Technology, Yangzhou University, Yangzhou, 225002, People's Republic of China

² Center for Multidimensional Carbon Materials, Institute for Basic Science (IBS), Ulsan 44919, Republic of Korea

³ Department of Materials Science and Engineering, Ulsan National Institute of Science and Technology (UNIST), Ulsan 44919, Republic of Korea

E-mail: xyzhang@yzu.edu.cn and f.ding@unist.ac.kr

Received 24 July 2018, revised 26 August 2018

Accepted for publication 12 September 2018

Published 1 October 2018



CrossMark

Abstract

The structure and stability of molecular junctions, which connect two single-wall carbon nanotubes (SWCNTs) of different diameters and chiral angles, (n_1, m_1) - (n_2, m_2) , are systematically investigated by density functional tight binding calculations. More than 100 junctions, which connect well-aligned SWCNTs, were constructed and calculated. For a highly stable junction between two chiral (n_1, m_1) and (n_2, m_2) SWCNTs with opposite handedness, the number of pentagon–heptagon (5/7) pairs required to build the junction can be denoted as $||n_2 - n_1| - |m_2 - m_1|| + \min\{|n_2 - n_1|, |m_2 - m_1|\}$ with (n_2, m_2) rotating $\pi/3$ angle or not. While for a junction connected by two zigzag, armchair or two chiral SWCNTs with the same handedness, the number of 5/7 pairs is equal to $|n_1 - n_2| + |m_1 - m_2|$. Similar to the formation energies of grain boundaries in graphene, the curve of the formation energies vs. chiral angle difference present an ‘M’ shape indicating the preference of ~ 30 degree junctions. Moreover, the formation energies of the zigzag-type and armchair-type junctions with zero misorientation angles are largely sensitive to the diameter difference of two sub-SWCNTs.

Supplementary material for this article is available [online](#)

Keywords: carbon nanotube junctions, pentagon–heptagon pairs, stabilities, misorientation angle, diameter

(Some figures may appear in colour only in the online journal)

1. Introduction

Single-wall carbon nanotubes (SWCNTs), cylindrical structures that can be obtained by rolling a graphene sheet, have attracted a great level of interest due to their novel properties and immense potential applications [1–6]. For example, the electronic properties of a SWCNT are largely determined by its diameter and chirality, indicated by a pair of chiral indexes (n, m) [7, 8]. An SWCNT with the (n, m) satisfying $n - m = 3i$ (i is integer) are metallic, while others are semiconducting [9]. Fusing two SWCNTs of different structures will inevitably introduce a

junction in the interface and, depending on the types of the two SWCNTs, the junction might be one of the three possible types, S–S, M–M or S–M, where S and M represent semiconducting and metallic SWCNTs, respectively, and the junctions of different types can be used as building blocks for various applications in future microelectronic devices [10–32].

Hitherto, great efforts have been made to explore the geometric structures of different tube–tube junctions, such as the bending tube–tube junctions, the junctions formed by fusing two SWCNTs, and so on [10–20]. During SWCNT growth, it was found that the chirality of a SWCNT might be changed and therefore such junctions could be frequently observed [21, 33]. Another method to produce SWCNTs with

⁴ Authors to whom any correspondence should be addressed.

well-aligned junctions is to transform the carbon nanopeapods into double walled CNTs (DWCNTs), during which the further fusion of the short SWCNTs formed by the fusion of fullerenes must lead to the formation of junctions in a long and straight mode in the inner wall SWCNTs [34, 35]. In addition, massive multiwall CN_x /carbon nanotube intramolecular junctions were also successfully fabricated by ordinary CVD method [36, 37].

Because of the great interests in the junctions in SWCNTs, many theoretical efforts have been made to explore their structures, properties and stabilities [14–16, 29, 30, 37–39]. While, a systematic theoretical study has not been available until now. Since the junctions connecting two straight SWCNTs are of high importance for SWCNT growth and electronic applications, in this study, we focus on the straight SWCNT junctions to explore the formation of highly stable junctions and their dependence on the structures of the two SWCNTs on both sides.

2. Models of the tube–tube junctions and calculation methods

In order to create the highly stable tube–tube junctions, we first place two SWCNTs, noted as T_1 and T_2 hereafter, together with their axes aligned with each other. Then all the dangling bonds at the junction of the configurations are eliminated by adding or removing carbon atoms to maintain a sp^2 -hybridized carbon network (figures 1(a)–(c)). Finally, the constructed junction was further annealed by rotating the randomly selected C–C bonds around the junction while the alignment of both tubes remains in order to locate the structure with the minimum formation energy. The method of tube–tube junction annealing was same as that shown in previous study [40]. According to the chiral structures of the two SWCNTs on both sides of the junction, three kinds of junctions are considered: Z–Z junctions which connect two zigzag (ZZ) SWCNTs (figure 1(f)), A–A junctions between two armchair (AM) SWCNTs (figure 1(g)) and C–C junctions connecting two SWCNTs with arbitrary chiral structures (figures 1(h)–(j)).

All the constituted SWCNTs used here can be projected on the map of figure 2. We divide the SWCNTs into two types of zones: (1) zone-I, where the SWCNT is right-handed (R) with the chiral angle in the range of $(0^\circ, 30^\circ)$, and (2) zone-II(1)/zone-II(2), where the SWCNT is left-handed (L) with the chiral angle in the range of $(30^\circ, 60^\circ)/(0^\circ, -30^\circ)$. Based on the handedness of two connected SWCNTs (figures 1(d), (e)), the C–C junctions are classified into three groups:

- (i) Symmetric junctions, $J-S$, between a right-handed (figure 1(d), zone-I in figure 2) and a left-handed (figure 1(e), zone-II(1), zone-II(2) in figure 2) SWCNT of mirror symmetries. Two SWCNTs have exactly same diameters ($R_1 = R_2$) but opposite chiral angles ($\theta_1 = -\theta_2$) and their chiral indexes can be written as (n, m) and (m, n) , respectively (figure 1(h)).

- (ii) Asymmetric junctions, $J-RR$ or $J-LL$ between two right-handed (zone-I in figure 2) or two left-handed (zone-II(1), zone-II(2) in figure 2) SWCNTs (figure 1(i)).
- (iii) Asymmetric junctions $J-LR$ or $J-RL$ between a right-handed (zone-I in figure 2) and a left-handed SWCNT (zone-II(1), zone-II(2) in figure 2), both have different diameters and different chiral angles (figure 1(j)).

To certify the asymmetric C–C SWCNT junctions are as straight as possible, we confine the diameters mismatch of two joint SWCNTs at less than 4%. Since most of the considered SWCNT junctions are quite large (some contain nearly 1000 atoms), density functional theory (DFT) calculations are too expensive for exploring more than 100 structures. We performed all the functional based tight binding (DFTB) theory as implemented in DFTB + code [41–43], which has been proved accurate enough for structure based calculations and much faster of DFT calculations. During all the structural optimizations, force convergence criterion was set as 10^{-4} Hartree/bohr. To examine the structural stabilities of the SWCNT junction, the formation energy (E_f) of a junction is defined as:

$$E_1 = (2 \times E_{T1} - E_{DT1})/2, \quad (1)$$

$$E_2 = (2 \times E_{T2} - E_{DT2})/2, \quad (2)$$

$$E_b = E_{T1} + E_{T2} - E_{junction}, \quad (3)$$

$$E_f = (E_1 + E_2 - E_b)/L, \quad (4)$$

where E_{T1} , E_{T2} , E_{DT1} , E_{DT2} and $E_{junction}$ are the energies of T_1 , T_2 , two longer tubes (DT_1 , DT_2) with same configurations as T_1 and T_2 but doublet lengths, and the structure with a junction between T_1 and T_2 , respectively. E_1 and E_2 are the formation energies of the open ends of T_1 and T_2 and E_b is the binding energy between the T_1 and T_2 after forming the tube–tube junction. $L = \pi (D_1 + D_2)/2$ is defined as the circumference length of the tube–tube junction and D_1 and D_2 are diameters of T_1 and T_2 , respectively.

3. Results and discussion

3.1. Structures and stabilities of Z–Z and A–A SWCNT junctions

To explore the Z–Z and A–A SWCNT junctions, we constructed heterostructures with six different chiral index combinations, $(n_1, 0) - (n_2, 0)$, $|n_1 - n_2| = 1, 2, 3$ and $(m_1, m_1) - (m_2, m_2)$, $|m_1 - m_2| = 1, 2, 3$. For each Z–Z SWCNT junctions, one or more pentagon–heptagon pairs (or the 5/7 dislocations), parallel to the tube axis (figures 3, 4(a)–(c), S1, S2 in the supporting information, SI is available online at stacks.iop.org/NANO/29/485702/mmedia), are formed at the interface of two ZZ SWCNTs. While for the optimum A–A SWCNT junctions, each 5/7 dislocation is no longer strictly parallel to the tube axis, instead, they are aligned with a small tilt angle to the tube axis (figures 4(d)–(f), S3–S5 in SI). Different from the tail-to-head orientated 5/7 pairs in graphene, the two parallel 5/7 pairs in such Z–Z or A–A SWCNT junctions interact repulsively with

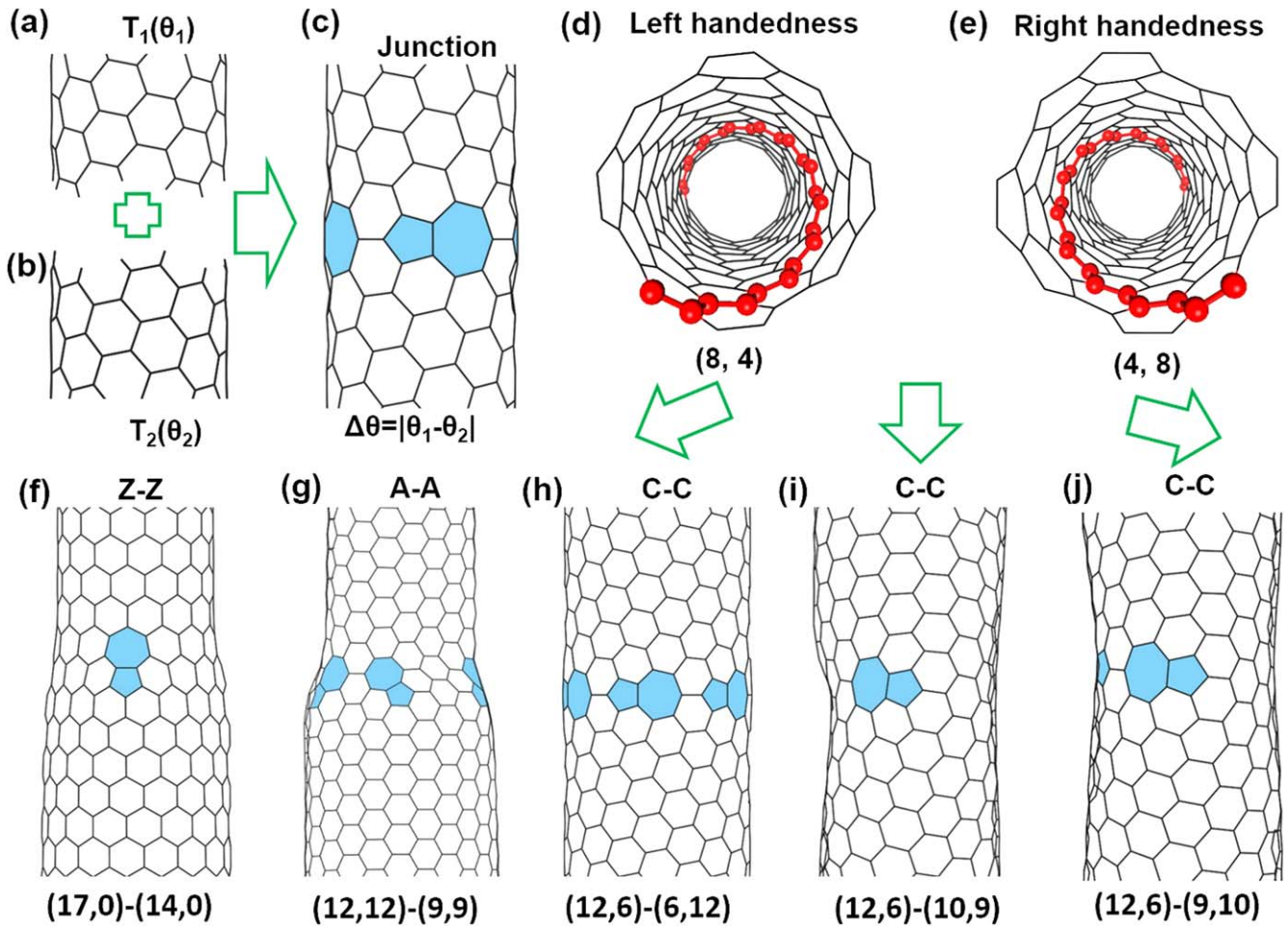


Figure 1. (a)–(c) Schematic diagrams of two SWCNTs (T_1 , T_2) and a fused SWCNT junction formed by welding them together, θ_1 , θ_2 and $\Delta\theta$ respects the chiral angle of T_1 , T_2 and their misorientation angle, respectively. (d), (e) the sketches of left-handed (L) (8, 4) and right-handed (R) (4, 8) SWCNTs. Atomic configurations of junctions between two zigzag SWCNTs (f), two armchair SWCNTs (g), two symmetric chiral SWCNTs with just opposite handedness (h) and two asymmetric chiral SWCNTs with same or opposite handedness (i), (j).

each other [44]. As shown in figures 3 and S5 in SI, with the two 5/7 pairs in (17,0)–(15,0) or (12,12)–(11,11) junction sitting closer with each other, the energy of the structure is largely increased. Therefore, all the Z–Z or A–A SWCNT junctions are constructed with evenly distributed 5/7 dislocations around the circles to certify the spacing between neighboring 5/7 dislocations as far as possible. Moreover, for any SWCNT junction, (n_1, m_1) – (n_2, m_2) , connected by two ZZ or AM carbon nanotubes in zone-I (see figure 2), the number of 5/7 dislocations is the lowest number of steps from (n_1, m_1) to (n_2, m_2) in the map, which can be expressed by equation (5):

$$|n_1 - n_2| + |m_1 - m_2| \quad (5)$$

Therefore, for a Z–Z SWCNT junction, the number of 5/7 dislocations is the same as the index difference of $|n_1 - n_2|$, that is, one, two and three pairs of 5/7 dislocations are created in the case of $|n_1 - n_2| = 1, 2, 3$, respectively. While for A–A SWCNT junctions, the number of the 5/7 pairs is $2|m_1 - m_2|$, that is, two, four and six 5/7 pairs are formed in the case of $|m_1 - m_2| = 1, 2, 3$, respectively.

The formation energies of all the constructed Z–Z/A–A SWCNT junctions are plotted in figures 4(g), (h). It is found that the formation energies increase with the number of 5/7

pairs for both types of junctions. Bond lengths analysis shows that the existence of more 5/7 pairs leads to a larger distortion to the sp^2 carbon network around the junction and therefore a resultant larger formation energy of the junction (see figures 4(i)–(n)). Moreover, for each type of Z–Z or A–A SWCNT junctions with same number of 5/7 pairs, their formation energy decreases with the diameters of constituent SWCNTs (figures 4(g), (h)). Compared with a thinner Z–Z/A–A SWCNT junction, the spacing between two neighboring 5/7 pairs in a fatter one with same number of 5/7 pairs is larger, which results in the decreased repulsive interaction and the lowered formation energy as well.

3.2. Structures and stabilities of C–C SWCNT junctions

3.2.1. Symmetric junctions (J–S) between two SWCNTs of opposite handednesses. According to the chirality of two SWCNTs, the misorientation angles ($\Delta\theta = |\theta_1 - \theta_2|$) of all the symmetric C–C SWCNT junctions are trapped in the period of $0^\circ \sim 60^\circ$. Different from the Z–Z and A–A SWCNT junctions, the 5/7 dislocations at a C–C SWCNT junction are head-to-tail aligned along the circumference of the junction (figures S5–S9 in SI), which is very similar to the formation of grain

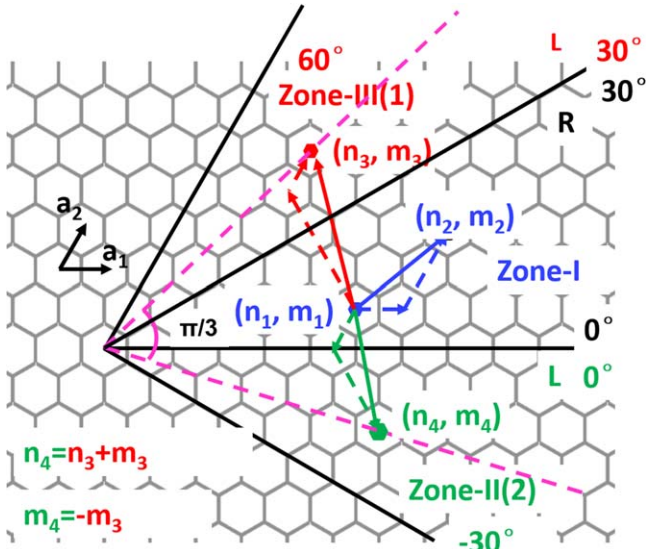


Figure 2. The map of (n_1, m_1) – (n_2, m_2) SWCNT junction connecting two sub-tubes of (n_1, m_1) and (n_2, m_2) at different zones (I, II(1), II(2)). In zone-I, the SWCNT is right-handed (R) with the chiral angle in the range of $(0^\circ, 30^\circ)$. In zone-II(1) and zone-II(2), the SWCNT is left-handed (L) with the chiral angle in the range of $(30^\circ, 60^\circ)$ and $(-30^\circ, 0^\circ)$, of which, one (n_3, m_3) SWCNT in zone-II(1) can be transformed to zone-II(2) as (n_4, m_4) by rotating $\pi/3$ angle.

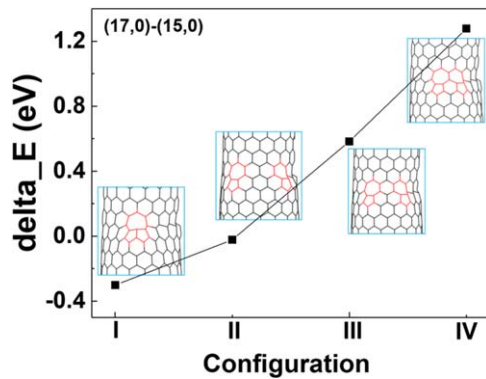


Figure 3. Energy differences of $(17, 0)$ – $(15, 0)$ Z–Z SWCNT junction with different arrangement of two $5/7$ dislocations. From configuration I to configuration IV, the spacing between two $5/7$ dislocations decreases sequentially.

boundaries (GBs) in graphene [37, 40–42]. According to the $5/7$ dislocations arrangements, the symmetric C–C SWCNT junctions can mainly be classified into three families:

- (I) C–C(1) J–Ss with $\Delta\theta$ in the range of $0^\circ \sim 21.79^\circ$ (figures 5(a)–(f), S6, S7 in SI), in which the $5/7$ defects at the interfaces are separated by one or more hexagons. With the increase of $\Delta\theta$, the line density of $5/7$ dislocations increase and the distance between neighboring $5/7$ pairs decreases (see figure 6(a)). At $\Delta\theta = 21.79^\circ$ (figure 5(f)), the separation between two adjacent $5/7$ dislocations remain only one hexagon [37, 41, 42].
- (II) C–C(2) J–Ss with $\Delta\theta$ in the range of $42.1^\circ \sim 60^\circ$, which is similar to the first family but the $5/7$ pairs sit a bit tilted with respect to the tube circumference direction

(figures 5(m)–(r), S8–S10 in SI). In contrast, the line density of $5/7$ pairs decrease with the increase of $\Delta\theta$ (see figure 6(a)) with the maximum at $\Delta\theta = 42.1^\circ$ (figure 5(m)), where two adjacent $5/7$ pairs are spaced by only one hexagon.

- (III) C–C(3) J–Ss with $\Delta\theta$ between 21.79° and 42.1° (figures S7, S8 in SI), in which some of the $5/7$ dislocations at the junction are tail-to-head connected with each other (see figure 6(a)). For example, the C–C J–S with 24.02° misorientation angle (figure 5(g)) has three isolated $5/7$ pairs and one fused $5/7$ – $5/7$ dislocations at the junctions. In the misorientation angle region of $21.79^\circ \leq \Delta\theta \leq 32.2^\circ$, the number of isolated $5/7$ dislocations decreases with $\Delta\theta$ while that of the consecutive $5/7$ dislocations increases (figure 6(a), S7(l), (m), S8(a)–(d) in SI). At $\Delta\theta = 32.2^\circ$ (figure 5(j)), the junction is completely constructed of continuous $5/7$ pairs. An opposite tendency is found in the range of $32.2^\circ \leq \Delta\theta \leq 42.1^\circ$, where the ratio of isolated $5/7$ dislocations increases while that of the consecutive ones decreases with the increase of the misorientation angles (figures 5(j)–(m), 6(a) and S8(e)–(j) in SI).

Similarly, for all the optimum C–C J–Ss, (n_1, m_1) – (n_3, m_3) , with sub-tubes in zone-I and zone-II(1) (figure 2), respectively, the number of $5/7$ dislocations is equivalent to the lowest number of steps from (n_1, m_1) to (n_3, m_3) or the equivalent counterpart (n_4, m_4) on the map, which can be summarized as:

$$\min \{ \|n_3 - n_1\| - |m_3 - m_1| + \min \{ |n_3 - n_1|, |m_3 - m_1| \}, |n_3 - n_1| + |m_3 - m_1| \} \quad (6)$$

or

$$\min \{ \|n_4 - n_1\| - |m_4 - m_1| + \min \{ |n_4 - n_1|, |m_4 - m_1| \}, |n_4 - n_1| + |m_4 - m_1| \} \quad (7)$$

where (n_4, m_4) is the equivalent counterpart of (n_3, m_3) by rotating $\pi/3$. For example, the number of $5/7$ dislocations for $(11,7)$ – $(7,11)$ and $(10,6)$ – $(6,10)$ are 4 and 4, respectively. While for $(10,1)$ – $(1,10)$ and $(15,3)$ – $(3,15)$, the number of $5/7$ dislocations becomes 2 and 6, respectively. It is found that linear density of $5/7$ dislocations increase linearly from 0° to 32.2° then decrease linearly to 60° (figure 6(a)).

Interestingly, the formation energies of these C–C J–Ss display an M-shape function with respect to their misorientation angles (see figure 6(d)). It is noted that the formation energies of these C–C J–Ss around the SWCNT circumferences per unit length are in the range of $0 \text{ eV}/\text{\AA} \sim 0.5 \text{ eV}/\text{\AA}$, similar to previous results for graphene GBs [43–46]. The smallest formation energy of $0 \text{ eV}/\text{\AA}$ at $\Delta\theta = 0^\circ$ and $\Delta\theta = 60^\circ$ refers to the defect free SWCNTs. The highest energy peak (**peak-I**) at the left panel of the energy curve appears at around $\Delta\theta = 17^\circ$, while at the right panel of the curve, the highest formation energy occurs (**peak-II**) at around $\Delta\theta = 44^\circ$. As for the C–C J–Ss with smaller $\Delta\theta$ than peak-I and larger $\Delta\theta$ than peak-II, a nearly

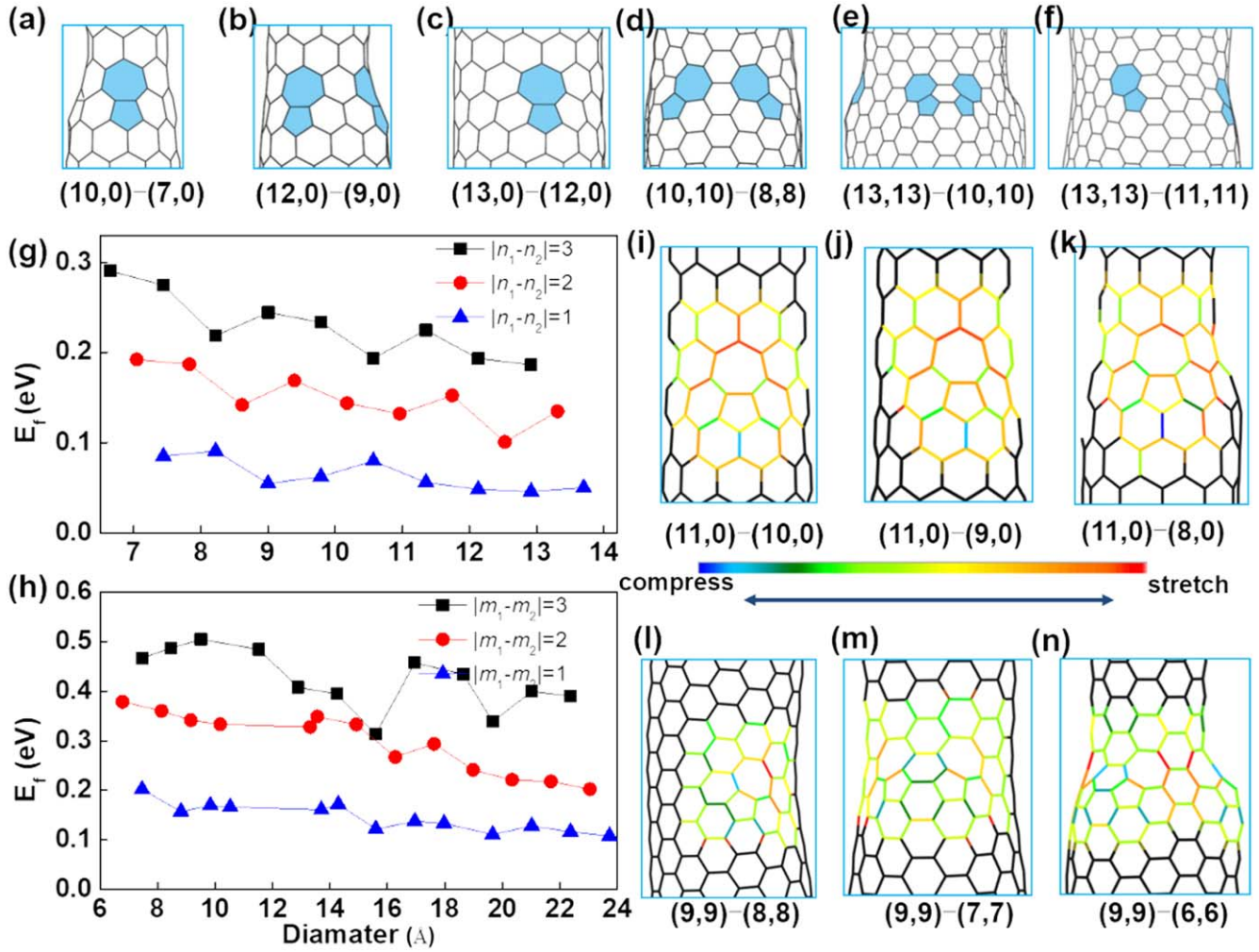


Figure 4. The geometries of three Z-Z (a)–(c) and three A-A SWCNT junctions (d)–(f). The formation energies (E_f) of Z-Z (g) and A-A SWCNT junctions (h) per unit length around the SWCNT circumferences. The black squares, red circles and blue triangles represent the formation energies at $|n_1 - n_2|/|m_1 - m_2| = 1, 2, 3$, respectively. Strain distributions around the 5/7 defects (colors from blue to red corresponding to the largest compression strain and the largest stretching strain) of three Z-Z (i)–(k) and three A-A (l)–(n) SWCNT junctions.

linear relationship of formation energy to $\Delta\theta$ is found, namely, the formation energies of C-C J-Ss increase from $\Delta\theta = 0^\circ$ to peak-I and decrease from peak-II to $\Delta\theta = 60^\circ$, respectively. While in the mediate misorientation angle region, the formation energies of C-C J-Ss decrease firstly and then increase almost linearly to peak-II with a local minimum locating at around $\Delta\theta = 32.2^\circ$.

Similar to the Z-Z/A-A SWCNT junctions, the 5/7 dislocations at the interface of C-C SWCNT junctions introduce extra strain and destabilizes the structures (see figures 6(g)–(l)). Conversely, the adjacent 5/7 dislocations at the junctions of chiral SWCNTs are attracted to each other, which can release the strain to some degree once they come together [43, 45, 47]. Therefore, the formation energies of such C-C SWCNT junctions can be simply evaluated by the equation (8):

$$\Delta E \sim \sum_i \varepsilon_{57,i} - \sum_i \varepsilon_{(5,i)(7,i+1)}, \quad (8)$$

where the $\varepsilon_{57,i}$ and $\varepsilon_{(5,i)(7,i+1)}$ items represent the strain energy caused by i th isolated 5/7 dislocation and the strain energy

caused by the fusion of adjacent pentagons and heptagons (figure S11(a) in SI). In the C-C(1) J-Ss ($\sim 0^\circ \leq \Delta\theta \leq 21.79^\circ$) and C-C(2) J-Ss ($\sim 42.1^\circ \leq \Delta\theta \leq 60^\circ$), the strains applied on the junctions are caused mainly by isolated 5/7 dislocations (see figure S11(a) in SI), therefore, the formation energies of such C-C SWCNT junctions are almost proportional to the line density of 5/7 dislocations (the first item of equation (8)). In contrast to the C-C(1) J-Ss, the projection density of 5/7 pairs around the SWCNTs circumference is a bit larger in those C-C(2) J-Ss (see figures 5(a)–(f), (m)–(r)), which causes the energy curve reach the peak-I on the left panel a bit larger than the peak-II on the right panel (see figure 6(d)). While for C-C(3) J-Ss ($\sim 21.79^\circ \leq \Delta\theta \leq 42.1^\circ$), the line density of head-to-tail 5/7 connections increase first and then decrease with the maximum at around $\Delta\theta = 32.2^\circ$ (see figure 6(a)). In this region, the strains induced by isolated 5/7 dislocations are offset in some degree due to the appearance of two or more adjacent 5/7 dislocations connecting (see figures 6(a), S11(b) in SI), as a result, the formation energies of the systems are moderately decreased as the second item of equation (8) is no longer zero. A local

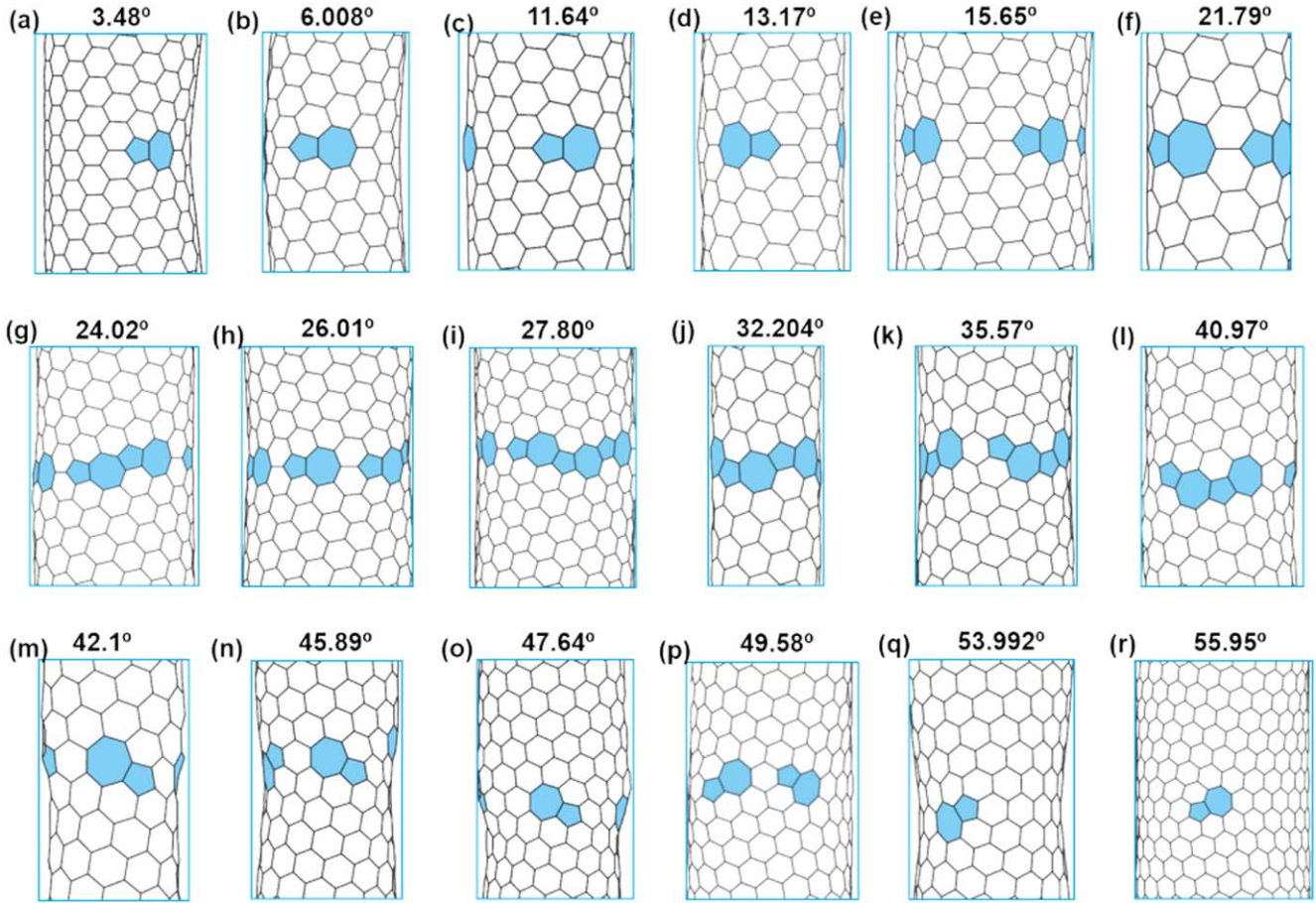


Figure 5. Optimum structures of (a)–(f) type-I, (g)–(l) type-III, and (m)–(r) type-II C–C J-Ss.

minimum appears at $\Delta\theta = 32.2^\circ$, the head-to-tail 5/7 connection at the interface offset the strain on the pentagon or heptagon in largest degree and leads to a largest reduction of formation energy at the energy curve. Based on the discussion, we can fit the formation energies in equations (9) and (10):

$$E_f = (3.57^* \rho_{57\text{iso}} - 2.33^* \rho_{57\text{con}}) \text{eV} \quad (\sim 0^\circ \leq \Delta\theta \leq 32.2^\circ) \quad (9)$$

$$E_f = (3.11^* \rho_{57\text{iso}} - 1.87^* \rho_{57\text{con}}) \text{eV} \quad (\sim 32.2^\circ \leq \Delta\theta \leq 60^\circ) \quad (10)$$

where 3.57 eV and 3.11 eV respect the formation energy of isolated 5/7 dislocation of C–C(1) J–Ss and C–C(2) J–Ss, respectively, and the 2.33 eV and 1.87 eV respects the decrease information energy when two 5/7 dislocations meet together. $\rho_{57\text{iso}}$ and $\rho_{57\text{con}}$ is the linear density of isolated 5/7 dislocations and their connections, respectively. It can be seen that the equations (9) and (10) well describe the evolution of formation energies of the C–C J–Ss (green line in figure 6(d)).

3.2.2. Asymmetric C–C J–RR(J–LL) and J–RL(J–LR). To reach a general view on the structural and energetic character of C–C SWCNT junctions, a number of asymmetric J–RRs(J–LLs) and J–RLs(J–LRs) are also extended (figures S12–S22 in SI). Due to the chirality limit of the SWCNTs with same handedness (L–L or R–R), the misorientation angles for J–RRs(J–LLs)

are only in the range of $0^\circ \sim 30^\circ$. Different from the C–C J–Ss, the mismatch of the diameters between two sub-SWCNTs here make the geometries of those J–RRs(J–LLs) and J–RLs(J–LRs) a bit complicate, where some irregular 5/7 pairs with a larger tilt angle (to the line around the tube circumference) appear. For example, some discrete C–C(2)-style 5/7 pairs appear in the smaller misorientation angle region ($0^\circ \leq \Delta\theta < 21.79^\circ$) due to the nonuniform structures. Besides, a tail-to-head 5/7 connection can be found even in the smaller ($0^\circ \leq \Delta\theta < 21.79^\circ$) and larger misorientation angle region ($42.1^\circ \leq \Delta\theta < 60.0^\circ$) (see figures S17, S18 in SI). As a result, even for same $\Delta\theta$, different topological structures are found between the symmetric and asymmetric C–C SWCNT junctions. Similar to the C–C J–Ss, the number of 5/7 pairs of J–RLs(J–LRs) can be counted by equation (6), which increase linearly in the range of around $0^\circ \leq \Delta\theta < 32^\circ$, but decrease linearly to $\Delta\theta = 60^\circ$. Moreover, the formation energies display a M-shape relationship to the misorientation angles, which the peak on the left and right panel of the energy profile are around $\Delta\theta = 17^\circ$ and 44° , respectively, leaving the local minimum around $\Delta\theta = 32^\circ$ (figure 6(e)). While for those asymmetric J–RRs(J–LLs), the largest formation energy appears at around $\Delta\theta = 19^\circ$ (figure 6(f)) and the number of 5/7 dislocations can be counted by equation (5). Importantly, the formation energies of these asymmetric SWCNT junctions can also be well

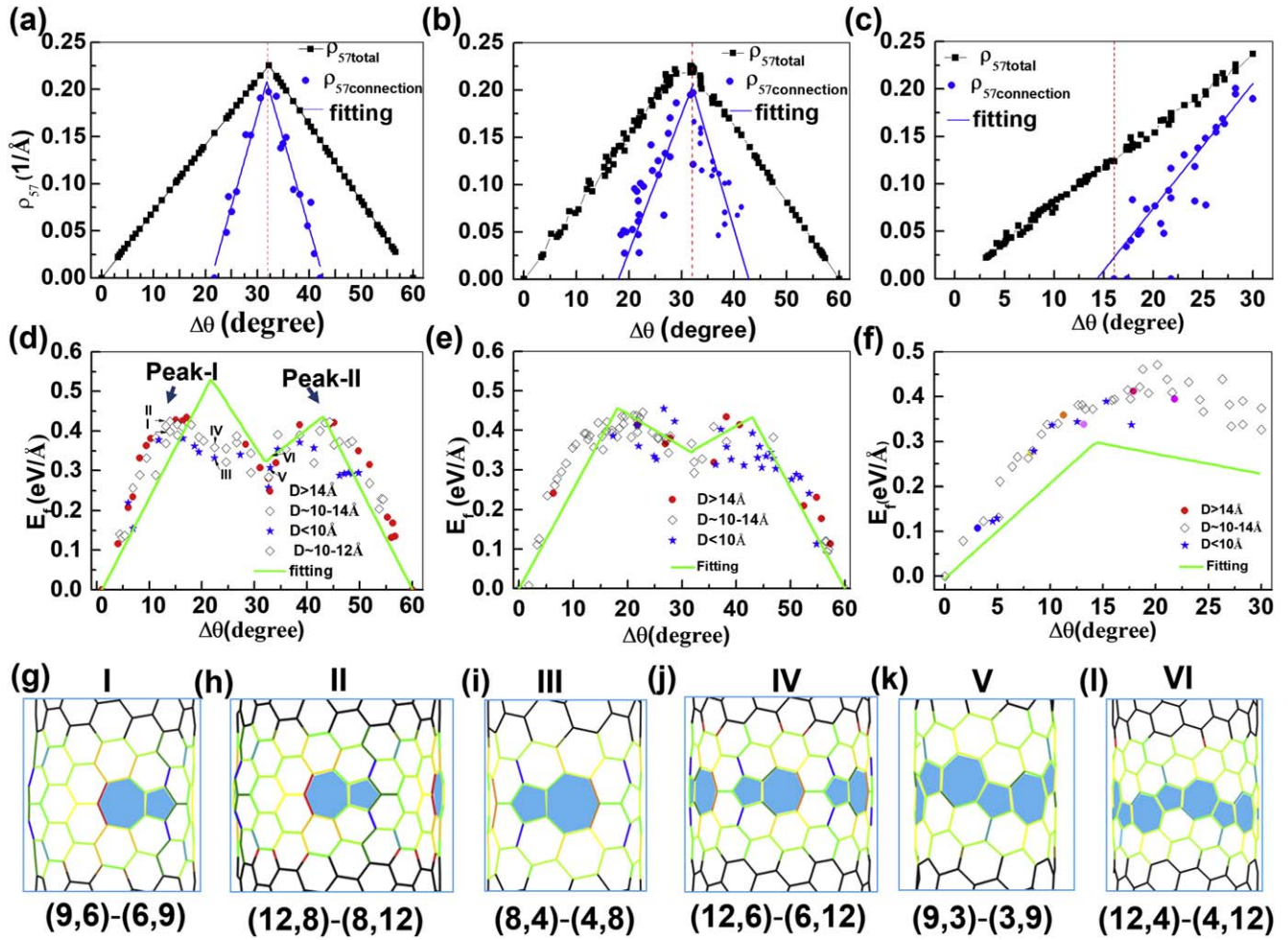


Figure 6. (a)–(c) The linear density of 5/7 dislocations and (d)–(f) the formation energies of C–C J–Ss and asymmetric J–LRs(J–RLs) and J–RRs(J–LLs) related to $\Delta\theta$ in the range of $0^\circ\sim 60^\circ$. The line respects the fitted results of 5/7 densities and formation energies, of which, $\rho_{5/7\text{total}}$ is the 5/7 dislocations density of the total system, and the $\rho_{5/7\text{con}}$ refers to the line density of head-to-tail connective 5/7 dislocations; (g–l) strain distributions around the 5/7 dislocations (colors from blue to red corresponds to the largest compression strain and the largest stretching strain) of six C–C J–Ss.

described by equations (9) and (10) (see the fitted lines in figures 6(e), (f)), respectively.

3.2.3. Diameter dependent stabilities of C–C SWCNT junctions. Furthermore, for the C–C SWCNT junctions with same misorientation angles, their formation energies are found to slightly increase with the diameters of the constituent SWCNTs (figures 6(g)–(l), S11(c) in SI), which is just in opposite tendency with that of Z–Z and A–A SWCNT junctions. For example, with same misorientation angle ($\Delta\theta = 13.17^\circ$) and 5/7 dislocation line density, the thinner (9, 6)–(6, 9) J–S (see figure 6(g)) has relatively smaller formation energy (~ 0.413 eV/Å) than the larger (12, 8)–(8, 12) J–S (~ 0.425 eV/Å) (see figure 6(h)). Similar energetic characters are found for (8, 4)–(4, 8) (figure 6(i)) J–S vs (12, 6)–(6, 12) J–S (figure 6(j)) and (9, 3)–(3, 9) (figure 6(k)) J–S vs (12, 4)–(4, 12) J–S (figure 6(l)). In figure S11(d) in SI, we plot the diagrams of two symmetric C–C J–Ss with same misorientation angle ($\Delta\theta$) but different diameters (the bigger circle and smaller circle). The number of 5/7 pairs is two and

three (blue short lines), and the intersection angle (α) between the tangent lines of two neighboring 5/7 pairs is $\alpha_1 = 90^\circ$ and $\alpha_2 = 120^\circ$, respectively. Unlike the Z–Z and A–A SWCNT junctions, the 5/7 pairs in such C–C J–Ss orientate along the perimeter of SWCNTs, thus, the strain caused by 5/7 pairs here can be averaged by the curvature of tube walls. As shown in figure S11(d) in SI, the curvature of thinner tube is a bit larger than that of the fatter one, which leads to the larger offset of the structural deformation and smaller formation energy for the former.

4. Conclusions

We systematically study the structures and stabilities of various one-dimensional mixed (n_1, m_1) – (n_2, m_2) SWCNT junctions consisting of two different chiral carbon nanotubes by density functional tight binding methods. For the straight Z–Z $[(n_1, 0) - (n_2, 0)]$, A–A $[(m_1, m_1) - (m_2, m_2)]$ SWCNT junctions and those C–C SWCNTs, $(n_1, m_1) - (n_2, m_2)$, with the sub-tubes of same handedness, the number of 5/7 pairs is

equal to the different index value of $|n_1 - n_2| + |m_1 - m_2|$. While for the C–C SWCNT junctions with the sub-tubes having opposite handedness, the number of 5/7 dislocations is the lowest number of steps between (n_1, m_1) to (n_2, m_2) and (n_1, m_1) to (n_2', m_2') , which (n_2', m_2') is equivalent to (n_2, m_2) by only rotating $\pi/3$ angle. Moreover, regularly organized 5/7 pairs around the circumferences are found on those C–C J–Ss, contrast to the organized 5/7 pairs for those asymmetric junctions. For Z–Z and A–A SWCNT junctions, their formation energies increase with a diameter difference of the two constituent nanotubes, but have opposite dependence with respect to the tube diameters. Most interestingly, an M-shape formation energy tendency is found for the C–C SWCNT junctions consisting of SWCNTs with similar diameters. Besides, the stabilities of the C–C SWCNT junctions with the same misorientation angles are found to increase with the diameters of the two-side SWCNTs. In future studies, the structures and stabilities of other carbon nanotube-based intramolecular junctions, such as the massive multiwall CN_x /carbon nanotube intramolecular junctions are expected to be explored.

Acknowledgments

The authors acknowledge the support of national science funding of China (NSFC) grants (Nos. 11574262, 21273189) and the Natural Science Foundation of the Jiangsu Higher Education Institutions of China (Grant No. 15KJB510031).

ORCID iDs

Xiuyun Zhang  <https://orcid.org/0000-0001-9977-4273>

References

- [1] Iijima S and Ichihashi T 1993 Single-shell carbon nanotubes of 1 nm diameter *Nature* **363** 603
- [2] Liu C, Fan Y Y, Liu M, Cong H T, Cheng H M and Dresselhaus M S 1995 Hydrogen storage in single-walled carbon nanotubes at room temperature *Science* **286** 1127
- [3] Dai H J, Hafner J H, Rinzler A G, Colbert D T and Smalley R E 1996 Nanotubes as nanoprobe in scanning probe microscopy *Nature* **384** 147
- [4] Sun P, Jiang Y D, Xie G Z, Du X S, Li X and Hu J 2011 Layer-by-layer assembly carbon nanotubes thin film based gas sensors for ammonia detection *J. Sci China Inform. Sci.* **54** 2680
- [5] Wu Z C *et al* 2004 Transparent, conductive carbon nanotube films *Science* **305** 1273
- [6] He M S *et al* 2017 Linking growth mode to lengths of single-walled carbon nanotubes *Carbon* **113** 231
- [7] Wildoer J W G, Venema L C, Rinzler A G, Smalley R E and Dekker C 1998 Electronic structure of atomically resolved carbon nanotubes *Nature* **391** 59
- [8] Odom T W, Huang J L, Kim P and Lieber C M 1998 Atomic structure and electronic properties of single-walled carbon nanotubes *Nature* **391** 62
- [9] Saito R, Fujita M, Dresselhaus G and Dresselhaus M S 1992 Electronic structure of chiral graphene tubes *Appl. Phys. Lett.* **60** 2204
- [10] Saito R, Dresselhaus G and Dresselhaus M S 1996 Tunneling conductance of connected carbon nanotubes *Phys. Rev. B* **53** 2044
- [11] Ebbesen T W and Takada T 1995 Topological and sp^3 defect structures in nanotubes *Carbon* **33** 973
- [12] Yao Z, Postma H W C, Balents L and Dekker C 1999 Carbon nanotube intramolecular junctions *Nature* **402** 273
- [13] Chico L, Crespi V H, Benedict L X, Louie S G and Cohen M L 1996 Pure carbon nanoscale devices: nanotube heterojunctions *Phys. Rev. Lett.* **76** 971
- [14] Koltai J, Ruzsnyak A, Zolyomi V, Kurti J and Laszlo I 2009 Junctions of left- and right-handed chiral carbon nanotubes–nanobamboo *Phys. Status Solidi b* **246** 2671
- [15] Han J, Anantram M P, Jaffe R L, Kong J and Dai H 1998 Observation and modeling of single-wall carbon nanotube bend junctions *Phys. Rev. B* **57** 14983
- [16] Charlier J C, Ebbesen T W and Lambin P 1996 Structural and electronic properties of pentagon-heptagon pair defects in carbon nanotubes *Phys. Rev. B* **53** 11108
- [17] Son Y W, Lee S B, Lee C K and Ihm J 2005 Electronic structure of straight semiconductor-semiconductor carbon nanotube junctions *Phys. Rev. B* **71** 205422
- [18] Wu G and Dong J M 2006 Raman characteristic peaks induced by the topological defects of carbon nanotube intramolecular junctions *Phys. Rev. B* **73** 245414
- [19] Lee G D, Wang C Z, Yu J, Yoon E, Hwang N M and Ho K M 2007 Formation of carbon nanotube semiconductor-metal intramolecular junctions by self-assembly of vacancy defects *Phys. Rev. B* **76** 165413
- [20] Menon M and Srivastava D 1997 Carbon nanotube ‘T junctions’: nanoscale metal-semiconductor-metal contact devices *Phys. Rev. Lett.* **79** 4453
- [21] Yao Y G *et al* 2007 Temperature-mediated growth of single-walled carbon-nanotube intramolecular junctions *Nat. Mater.* **6** 283
- [22] Li J, Papadopoulos C and Xu J 1999 Nanoelectronics: growing Y-junction carbon nanotubes *Nature* **402** 253
- [23] Papadopoulos C, Rakitin A, Li J, Vedenev A S and Xu J M 2000 Electronic transport in Y-junction carbon nanotubes *Phys. Rev. Lett.* **85** 3476
- [24] Satishkumar B C, Thomas P J, Govindaraj A and Rao C N R 2000 Y-junction carbon nanotubes *Appl. Phys. Lett.* **77** 2530
- [25] Andriotis A N, Menon M, Srivastava D and Chernozatonskii L 2001 Rectification properties of carbon nanotube ‘Y-junctions’ *Phys. Rev. Lett.* **87** 066802
- [26] Chiu P W, Kaempgen M and Roth S 2004 Band-structure modulation in carbon nanotube T junctions *Phys. Rev. Lett.* **92** 246802
- [27] Wei D C and Liu Y Q 2008 The intramolecular junctions of carbon nanotubes *Adv. Mater.* **20** 2815
- [28] Park J, Daraio C, Jin S, Bandaru P R, Gaillard and Rao A M 2006 Three-way electrical gating characteristics of metallic Y-junction carbon nanotubes *Appl. Phys. Lett.* **88** 243113
- [29] He L, Lu J Q and Jiang H Q 2009 Controlled carbon–nanotube junctions self-assembled from graphene nanoribbons *Small* **5** 2802
- [30] Martin-Martinez F J, Melchor S and Dobado J A 2011 Causes of energy destabilization in carbon nanotubes with topological defects *Theor. Chem. Acc.* **128** 445
- [31] Xiang D, Wang X L, Jia C, Lee T and Xuefeng Guo X 2016 Molecular-scale electronics: from concept to function *Chem. Rev.* **116** 4318

- [32] Wang L, Wang L, Zhang L and Xiang D 2017 Advance of mechanically controllable break action for molecular electronics *Top. Curr. Chem.* **375** 61
- [33] Yao Y G, Dai X C, Liu R, Zhang J and Liu Z F 2009 Tuning the diameter of single-walled carbon nanotubes by temperature-mediated chemical vapor deposition *J. Phys. Chem. C* **113** 13051
- [34] Smith B W, Monthieux M and Luzzi D E 1998 Encapsulated C₆₀ in carbon nanotubes *Nature* **396** 323
- [35] Smith B W, Monthieux M and Luzzi D E 1999 Carbon nanotube encapsulated fullerenes: a unique class of hybrid materials *Chem. Phys. Lett.* **315** 31
- [36] Chai Y, Zhou X L, Li P J, Zhang W J, Zhang Q F and Wu J L 2005 Nanodiode based on a multiwall CN_x/carbon nanotube intramolecular junction *Nanotechnology* **16** 2134
- [37] Chai Y, Zhang Q F and Wu J L 2006 A simple way to CN_x/carbon nanotube intramolecular junctions and branches *Carbon* **44** 687
- [38] Kim H *et al* 2003 Direct observation of localized defect states in semiconductor nanotube junctions *Phys. Rev. Lett.* **90** 216107
- [39] Pan B C, Yang W S and Yang J L 2000 Formation energies of topological defects in carbon nanotubes *Phys. Rev. B* **62** 12652
- [40] Zhang X Y, Xu Z W, Yuan Q H, John H and Ding F 2015 The favourable large misorientation angle grain boundaries in graphene *Nanoscale* **7** 20082
- [41] Porezag D, Frauenheim T, Kohler T, Seifert G and Kaschner R 1995 Construction of tight-binding-like potentials on the basis of density-functional theory: application to carbon *Phys. Rev. B* **51** 12947
- [42] Elstner M *et al* 1998 Self-consistent-charge density-functional tight-binding method for simulations of complex materials properties *Phys. Rev. B* **58** 7260
- [43] Koskinen P and Makinen V 2009 Density-functional tight-binding for beginners *Comp. Mater. Sci.* **47** 237
- [44] Yakobson B I and Ding F 2011 Observational geology of graphene, at the nanoscale *ACS Nano* **5** 1569
- [45] Xu Z W, Li H, Fujisawa K, Kim Y A, Endo M and Ding F 2012 Multiple intra-tube junctions in the inner tube of peapod-derived double walled carbon nanotubes: theoretical study and experimental evidence *Nanoscale* **4** 130
- [46] Liu T H, Gajewski G, Pao C W and Chang C C 2011 Structure, energy, and structural transformations of graphene grain boundaries from atomistic simulations *Carbon* **49** 2306
- [47] Yazyev O V and Louie S G 2010 Topological defects in graphene: Dislocations and grain boundaries *Phys. Rev. B* **81** 195420